Neurobiology of Disease 114 (2018) 65–73

Contents lists available at ScienceDirect

Neurobiology of Disease

journal homepage: www.elsevier.com/locate/ynbdi

Abnormal hippocampal theta and gamma hypersynchrony produces network and spike timing disturbances in the *Fmr1*-KO mouse model of Fragile X syndrome

Tara Arbab[a,b,c,*], Francesco P. Battaglia[a,d], Cyriel M.A. Pennartz[a,e,1], Conrado A. Bosman[a,e,**,1]

[a] Cognitive & Systems Neuroscience, Swammerdam Institute, Center for Neuroscience, Faculty of Science, University of Amsterdam, Sciencepark 904, 1098 XH Amsterdam, The Netherlands
[b] Netherlands Institute for Neuroscience, Institute of the Royal Netherlands Academy of Arts and Sciences, Meibergdreef 47, 1105 BA Amsterdam, The Netherlands
[c] Department of Psychiatry, Academic Medical Center, University of Amsterdam, Postal Box 22660, 1100 DD Amsterdam, The Netherlands
[d] Donders Institute for Brain, Cognition, and Behaviour, Radboud Universiteit Nijmegen, Heyendaalseweg 135, 6525 AJ Nijmegen, The Netherlands
[e] Research Priority Program Brain and Cognition, University of Amsterdam, Postal Box 94216, 1090 GE Amsterdam, The Netherlands

ARTICLE INFO

Keywords:
Fragile X syndrome
Hippocampus
Neuronal network activity
Spike-field coherence
Gamma oscillations
Theta oscillations

ABSTRACT

Neuronal networks can synchronize their activity through excitatory and inhibitory connections, which is conducive to synaptic plasticity. This synchronization is reflected in rhythmic fluctuations of the extracellular field. In the hippocampus, theta and gamma band LFP oscillations are a hallmark of the processing of spatial information and memory. Fragile X syndrome (FXS) is an intellectual disability and the most common genetic cause of autism spectrum disorder (Belmonte and Bourgeron, 2006).

Here, we investigated how neuronal network synchronization in the mouse hippocampus is compromised by the *Fmr1* mutation that causes FXS (Santos et al., 2014), relating recently observed single-cell level impairments (Arbab et al., 2017) to neuronal network aberrations. We implanted tetrodes in hippocampus of freely moving *Fmr1*-KO and littermate wildtype (WT) mice (Mientjes et al., 2006), to record spike trains from multiple, isolated neurons as well as LFPs in a spatial exploration paradigm.

Compared to wild type mice, *Fmr1*-KO mice displayed greater power of hippocampal theta oscillations, and higher coherence in the slow gamma band. Additionally, spike trains of *Fmr1*-KO interneurons show decreased spike-count correlations and they are hypersynchronized with theta and slow gamma oscillations. The hypersynchronization of *Fmr1*-KO oscillations and spike timing reflects functional deficits in local networks. This network hypersynchronization pathologically decreases the heterogeneity of spike-LFP phase coupling, compromising information processing within the hippocampal circuit. These findings may reflect a pathophysiological mechanism explaining cognitive impairments in FXS and autism, in which there is anomalous processing of social and environmental cues and associated deficits in memory and cognition.

1. Introduction

Fragile X syndrome (FXS) is a monogenic intellectual disability that shows behavioral overlap with autism spectrum disorder (ASD) (Belmonte and Bourgeron, 2006), accounting for an estimated 5% of its prevalence (Budimirovic and Kaufmann, 2011). FXS arises from a triplet expansion of the *Fmr1* gene, silencing expression of the fragile X mental retardation protein (FMRP). FMRP binds mRNAs encoding approximately one third of pre- and postsynaptic proteins, most significantly targeting those involved in synaptic signaling pathways involved in long-term potentiation (LTP) and depression (LTD), CREB signaling, glutamate receptor regulation, and GABA receptor mediated inhibition (Darnell et al., 2011; Bhakar et al., 2012). FMRP silencing effectively leads to disturbed synaptic function and plasticity of both interneurons and pyramidal cells (Santos et al., 2014; Pilpel et al., 2009).

FXS is a promising target for obtaining a multi-dimensional understanding from genes, to microcircuits and networks, to cognitive

* Correspondence to: T. Arbab, Netherlands Institute for Neuroscience, Institute of the Royal Netherlands Academy of Arts and Sciences, Meibergdreef 47, 1105 BA Amsterdam, The Netherlands.
** Correspondence to: C.A. Bosman, Research Priority Program Brain and Cognition, University of Amsterdam, Postal Box 94216, 1090 GE Amsterdam, The Netherlands.
E-mail addresses: t.arbab@nin.knaw.nl (T. Arbab), c.a.bosmanvittini@uva.nl (C.A. Bosman).
[1] These authors contributed equally to this manuscript.

https://doi.org/10.1016/j.nbd.2018.02.011
Received 22 November 2017; Received in revised form 12 February 2018; Accepted 21 February 2018
Available online 24 February 2018

impairment in neuropsychiatric disease due to its relatively simple genetic etiology (Fung and Reiss, 2016) and the development of rodent models (Mientjes et al., 2006; Berzhanskaya et al., 2017). Particularly affected in human patients and animal models is the hippocampus (Kates et al., 1997; Reiss et al., 1994), a structure essential for storing and consolidating experiences into long-term episodic and semantic memory.

Both animal (Kim and Fanselow, 1992; Morris et al., 1982) and human (Manns et al., 2003; Moscovitch et al., 2016) studies link the hippocampus to spatial, contextual, autobiographical and semantic memory. Single hippocampal neurons respond to the concept of given individuals, landmarks or objects (Quiroga et al., 2005). In FXS animal models, learning and memory deficits have been associated with dysfunction of the mechanisms underlying activity-dependent synaptic plasticity in the hippocampus (Bhakar et al., 2012; Huber et al., 2002).

Synaptic plasticity strongly depends on the precise temporal coordination of neuronal activity (Markram et al., 1997). This temporal coordination of neuronal activity is reflected in rhythmic oscillations of the local field potential (LFP) (Buzsáki et al., 2012). Neuronal oscillations have been associated with several cognitive and mechanistic processes through the brain, including neuronal communication and precise spike timing of activated neuronal groups (Bosman et al., 2014; Fries, 2015; Sejnowski and Paulsen, 2006). Hippocampal theta (4–8 Hz) chunks this experiential information in oscillation cycles (Skaggs and McNaughton, 1996; Gupta et al., 2012), and theta-nested gamma (20–100 Hz) oscillations induce synaptic plasticity, supporting memory consolidation processes (Bosman et al., 2014; Zheng et al., 2016; Colgin and Moser, 2010). Recently, abnormal gamma and theta phase-amplitude patterns of dendritic CA1 LFP oscillations were found in a mouse model of FXS (Radwan et al., 2016), related to an impaired excitatory-inhibitory equilibrium in FXS neuronal networks (Fenton, 2015; Contractor et al., 2015). However, it is unknown how these oscillatory dysfunctions affect the temporal coordination of spiking responses in these networks. Here, we hypothesize that compromised synaptic function in *Fmr1*-KO mice affects both the temporal coordination of cell ensembles and hippocampal oscillatory rhythms supporting neuronal synchronization. We evaluated this hypothesis using tetrode recordings the CA1 region of freely moving *Fmr1*-KO mice.

2. Material and methods

2.1. Subjects

We used four male *Fmr1*-KO (Mientjes et al., 2006) and four littermate wildtype (WT) control mice. All experiments were performed in accordance with Dutch National Animal Experiments regulations, were approved by the University of Amsterdam. Animals were received from the Erasmus MC Rotterdam breeding unit at an age of 8 weeks and group-housed until surgery. They were maintained on a regular 12-hour light-dark cycle (lights on: 8 am, lights off: 8 pm) and received water and food *ad libitum* throughout the experiment. To minimize bias due to possible undetected changes in environmental conditions, *Fmr1*-KO and WT animals were always studied in pairs; both recordings were done on the same day and counterbalanced per genotype. Therefore, the experimenter was not blind to genotype during the experiments: pairs of one *Fmr1*-KO and one WT mouse were implanted with a microdrive in each experiment. Once habituated to the experimenter and handling, mice underwent drive implantation surgery under buprenorphine-isoflurane anesthesia and were left to recover before the experiments.

2.2. Electrophysiological techniques

Six independently moveable tetrodes were loaded into a custom-made microdrive (Battaglia et al., 2009) and implanted over dorsal hippocampus (AP: −2.0 mm, ML: −2 mm; Fig. 1A). The tetrodes were advanced into the CA1 pyramidal cell layer guided by electrophysiological signals (sharp wave-ripple events) over the course of days following implantation surgery. Electrophysiological activity was recorded on an analog 27-channel Neuralynx data acquisition system at a 32 kHz sampling rate. Tetrode signals (bandpass filtered 0.6–6.0 kHz for single unit and 0.1–475 Hz for LFP) were referred to a nearby tetrode which was targeted to a location devoid of single unit activity. Single-unit data were preprocessed with Klustakwik (Harris et al., 2000) for automated spike clustering and the results were manually refined using Klusters (Hazan et al., 2006). The resulting spike trains were analyzed using custom-written MATLAB code. LFP analyses were done in MATLAB using FieldTrip (Oostenveld et al., 2011) and custom-made routines. Animal tracking position was extracted from video footage by Ethovision XT software (Noldus, Wageningen, the Netherlands) which was synchronized with the electrophysiological data

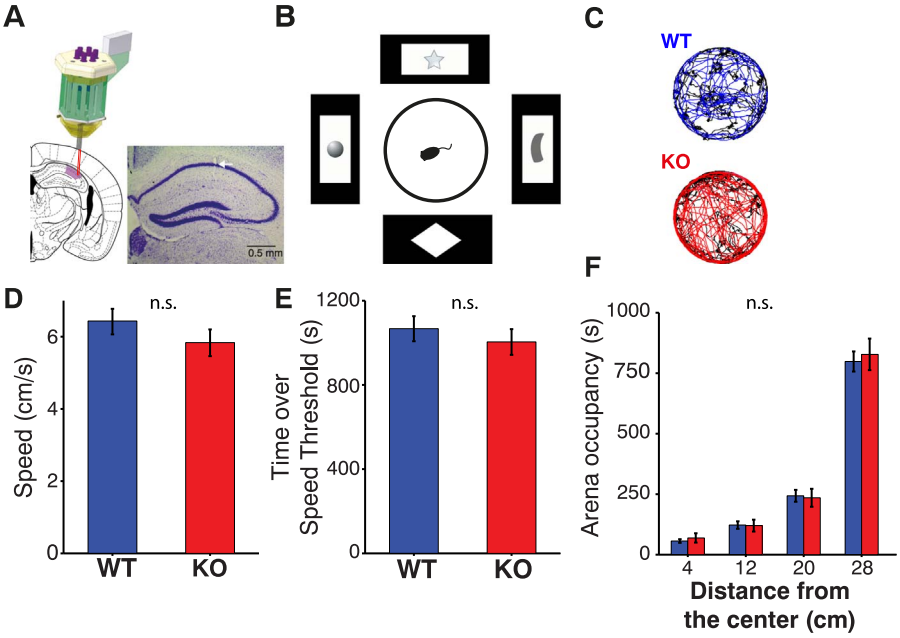

Fig. 1. Experimental setup and behavior.
(A) Left, Schematic of microdrive implantation target. Right, Coronal section showing the recording location (lesion) of a tetrode (arrow) in dorsal hippocampus CA1. (B) Schematic of the behavioral protocol. Animals freely explored a circular open field arena (middle) which was surrounded by four posters with geometric figures. (C) Accumulated trajectories of a WT (blue) and KO (red) animal exploring the arena during an example session in which the animal moved above threshold speed (3 cm/s). Inactivity periods (< 3 cm/s) are shown in black. (D) Average speed (> 3 cm/s) of WT and KO animals during arena exploration. (E) Average time per session where speed of WT and KO animals was > 3 cm/s. (F) Average time WT and KO animals spent at varying distances from the center of the arena (as a measure of thigmotaxis). Data (D–F) are represented as mean ± SEM.

acquisition system. At the end of experiments, electrolytic lesions were made to verify tetrode placement. Brains were fixed by transcardial perfusion and Nissl stained (Fig. 1A). Only animals with clear lesions in the CA1 pyramidal layer were included in the analysis.

2.3. Behavioral protocol

A full experiment consisted of four sessions (two per day on two consecutive days) during which hippocampal neuronal network activity was recorded as the mice freely explored a fully transparent, circular open field arena (diameter 64 cm) for 30 min. The arena was surrounded by black curtains and four large visual cues (Fig. 1B). In the final (fourth) session, three of the visual cues were removed. For the current analyses, we excluded this last session and pooled the others. The two daily recording sessions were separated by a two-hour break, during which the animal rested in its home cage. Each animal was used for multiple experiments; a new set of cues was selected for each experiment.

2.4. Analysis of neural data

Tracking of animal position was automated. For further control, however, tracking data were visually inspected, checked for accuracy, and corrected manually when necessary. Inactivity periods (animal speed < 3 cm/s) were excluded from analysis. Recording stability of individual neuronal clusters was examined; clusters whose first principal component exceeded more than three standard deviations from beginning to end of recording were excluded from analysis. Using a fuzzy clustering algorithm (Fuzzy Clustering and Data Analysis Toolbox, http://www.abonyilab.com/software-and-data/fclusttoolbox), the remaining clusters were separated in putative interneurons and pyramidal cells based on their firing rate and the mean width of their spike interval autocorrelograms (mean AC) (Lansink et al., 2010). The fuzzy clustering algorithm quantifies the certainty (*e.g.*, confidence level) that a neuron belongs to either group. Thus, neurons with a < 70% certainty of belonging to either group (unclassified) were excluded from analysis.

2.5. Spectral analysis

Power line artifacts of LFP raw traces were eliminated using a Discrete Fourier Transform (DFT) filter at 50 Hz and its 2nd and 3rd harmonic (Schoffelen et al., 2005). Each epoch of interest (where animal speed was > 3 cm/s), was centered in 10 s of the continuous signal. We then calculated the DFT of this 10 s epoch at 50 Hz, 100 Hz, and 150 Hz, and subtracted their respective sine waves from the continuous raw signal, with the amplitudes and phases as estimated by the respective DFTs. The epoch of interest (animal speed > 3 cm/s) was cut out from the cleaned 10 s epoch (Schoffelen et al., 2005). LFP segments containing artifacts were discarded from further analyses. Remaining data were *Z*-transformed to equalize the contribution of different tetrodes and sessions across animals. Raw LFP data was demeaned and divided by its standard deviation. Periods of animal activity (speed > 3 cm/s) were segmented in epochs of 1 s, Hanning tapered and Fourier transformed. Power estimates were normalized per session and animal relative to the mean power between 4 and 100 Hz (Malkki et al., 2016). An additional normalization to the maximum value of the averaged power spectrum across animals and sessions was used in Fig. 4A. Time-frequency estimates were calculated using a sliding window of 0.5 s with 95% overlap across the original segments. The average estimation over the first 4 s of activity in each segment is represented in Fig. 4B.

Coherence between LFP channels across different tetrodes was calculated using the weighted phase lag index (WPLI) (Vinck et al., 2011). The WPLI is a measure of phase-synchronization between LFP signals which is less affected by volume-conduction, noise and sample size. The WPLI was computed by:

$$\Phi = \frac{|E\{\Im\{X\}\}\, sgn(\Im\{X\})|}{E\{|\Im\{X\}|\}} \quad (1)$$

where $\Im\{X\}$ represents the imaginary part of the cross-spectrum between channels (Schoffelen et al., 2005). Normalized power and WPLI spectra were averaged across sessions and animals.

The consistency with which a cell fired spikes in a given phase range of an LFP oscillation was quantified using the pairwise phase consistency (PPC), a pairwise measure which is not biased by the number of spikes and non-Poissonian effects within spike trains (Vinck et al., 2010). Briefly, for each frequency f we determined spike-LFP phases in epochs of $2/f$ (2 cycles) length centered around each spike, in order to maintain the same resolution at any frequency bin. These segments were Fourier transformed using a Kayser taper ($\beta = 3$). The resulting complex arguments were used to quantify the PPC per cell and per frequency bin as follows:

$$\psi = \frac{\sum_{j=1}^{N_m} \sum_{k \neq j}^{N_m} (\sin(\theta_{j,m}) \sin(\theta_{k,m}) + \cos(\theta_{j,m}) \cos(\theta_{k,m}))}{N_m (N_m - 1)} \quad (2)$$

where $\theta_{,m}$ and $\theta_{k,m}$ are the jth and kth spikes at frequency f in trial m and N_m denotes the number of spikes N in trial m (Vinck et al., 2010). Additionally, we calculated the LFP spike-triggered average of ± 0.5 s segments around spikes.

2.6. Spike count correlations

The spike-count correlation (r_{SC}) measures the Pearson correlation between binned firing rate fluctuations of spike trains of two neurons (Cohen and Kohn, 2011; Averbeck and Lee, 2006; Kass et al., 2005). It is defined as:

$$r_{SC} = \frac{\sum_{n=1}^{N} (r_i^n - \bar{r}_i) \times (r_i^n - \bar{r}_j)}{\sigma_i \times \sigma_j} \quad (3)$$

where N is the number of trials and $r_n{}^i$ is the number of spikes of cell i in trial n over a specific spike-count window. The resulting spike-counts are z-scored using the mean spiking rate $\bar{r}_i$ and standard deviation of the firing rate of neuron i (σ_i) across sessions, to allow comparisons between different sessions and animals (Nandy et al., 2017). In our analyses, r_{SC} was calculated over a spike-count window of 0.5 s across data segments in which animals were active (speed > 3 cm/s). To control for trial-to-trial variability in spike-count correlation (Kass and Ventura, 2006), we repeated the spike-count correlation analysis through different spike-count windows, ranging from 0.05 to 1 s (Fig. 3C).

2.7. Statistical testing

Spike-count correlations and behavioral differences between genotypes were quantified using a Wilcoxon rank sum test, with a significance threshold of $p < 0.05$. Spectral estimates (Power, WPLI, Spike-LFP PPC) were tested across all frequencies for significance at a $p < 0.05$ level, using a nonparametric randomization test, corrected for multiple comparisons across frequencies (Bosman et al., 2012). We first calculated a spectral estimate across all epochs per genotype. Then, we calculated the T-statistic between genotypes for every frequency bin. Next, we performed 10,000 randomizations, in which: (Belmonte and Bourgeron, 2006) the epochs from both conditions were randomly redistributed; (Santos et al., 2014) from these two new random distributions, we calculated the T-statistics for every frequency bin; and (Arbab et al., 2017) the maxima and minima of these T-statistics were assigned to two distributions. These randomizations yielded two distributions of the 10,000 maximal and minimal differences between the randomly redistributed epochs. Finally, the experimentally observed T-statistics were compared to the maximal and minimal distributions. If differences were smaller than the 2.5th percentile of the minimal distribution or larger than the 97.5th percentile of the maximal

distribution, they were considered significant at a $p < 0.05$ level. This corresponds to a two-sided test with multiple comparison correction across frequencies (Maris et al., 2007; Nichols and Holmes, 2001). Effect sizes and p-values for genotypic differences were quantified using a Wilcoxon rank sum test over the average of the different frequency bands.

3. Results

Four *Fmr1*-KO (KO) (Mientjes et al., 2006) and four wild-type (WT) mice were implanted with six independently movable tetrodes in the CA1 pyramidal cell layer (Fig. 1A). Mice were habituated to an open field arena, surrounded by 4 different visual cues (Fig. 1B). The behavioral protocol consisted of three sessions of 30 min each, spread across 2 days, in which mice freely explored the arena. Altogether, mice were recorded over 69 sessions (WT: 34, KO: 35).

Both genotypes showed similar exploratory behavior across all recorded sessions. WT and KO mice ran indistinctly through the open arena (Fig. 1C). We did not observe significant differences in running speed (Fig. 1D: WT: 6.4 ± 0.4 cm/s, KO: 5.8 ± 0.4 cm/s, $p = 0.45$, Wilcoxon rank sum test). The amount of time the animal spent actively (> 3 cm/s) exploring the environment was similar in both genotypes (Fig. 1E: WT: 1067 ± 56.8 s, 1004 ± 59.3 s, $p = 0.26$, Wilcoxon rank sum test). Thigmotaxis, the tendency to remain in the periphery of the arena, did not differ between WT and KO mice either (Fig. 1F: WT: center 1975 ± 261 s, periphery $27.94 \times 10^3 \pm 1.45 \times 10^3$ s, $p < 0.001$; KO: center 2416 ± 675 s, periphery $28.97 \times 10^3 \pm 2.28 \times 10^3$ s, $p < 0.001$; comparison across genotypes, periphery, $p = 0.87$, Wilcoxon rank sum test). The lack of basic behavioral effects in this phenotypic characterization of the *Fmr1*-KO mice is in agreement with the mild behavioral effects of the *Fmr1* deletion observed elsewhere (Kazdoba et al., 2014).

Electrophysiological recordings were performed while mice freely explored the arena. We compiled and analyzed epochs in which running speed was above 3 cm/s. In both genotypes, CA1 LFP signals showed strong theta band (4 to 8 Hz) activity (Figs. 2A, 4A and B) with nested gamma (Fig. 2A), both features typical of mouse hippocampal LFP during motor activity (Buzsáki et al., 2003). We recorded approximately 6 neurons per recording session (381 neurons in total). Using a fuzzy clustering algorithm on the recorded neurons (Lansink et al., 2010), we identified 310 putative pyramidal neurons (152 for WT, 158 for KO) and 71 putative interneurons (WT: 36, KO: 35). Fig. 2B and C show the different waveforms obtained for both neuronal types and genotypes. Importantly, waveform parameters did not differ between genotypes. The fuzzy clustering algorithm allowed us to identify putative interneurons and pyramidal cells for both genotypes (Fig. 2B and C). We calculated three different waveform parameters: mean AC, Initial slope of valley decay (ISVD) (Lansink et al., 2010) and the peak-to-valley ratio for the previously identified neuronal types, separated by genotype (Table 1). We used a 2-way ANOVA test to reveal potential significant effects for neuronal type and genotype using these waveform parameters. We found a significant effect for mean AC and ISVD (but not for peak-to-valley ratio) for neuronal type (Mean AC: $F_{1,380} = 154.7$, $p < 0.001$; ISVD: $F_{1,350} = 12.08$, $p < 0.001$; peak-to-valley ratio: $F_{1,378} = 0.02$, $p = 0.93$). We did not find any significant effect for genotype (Mean AC: $F_{1,380} = 3.18$, $p = 0.08$; ISVD:

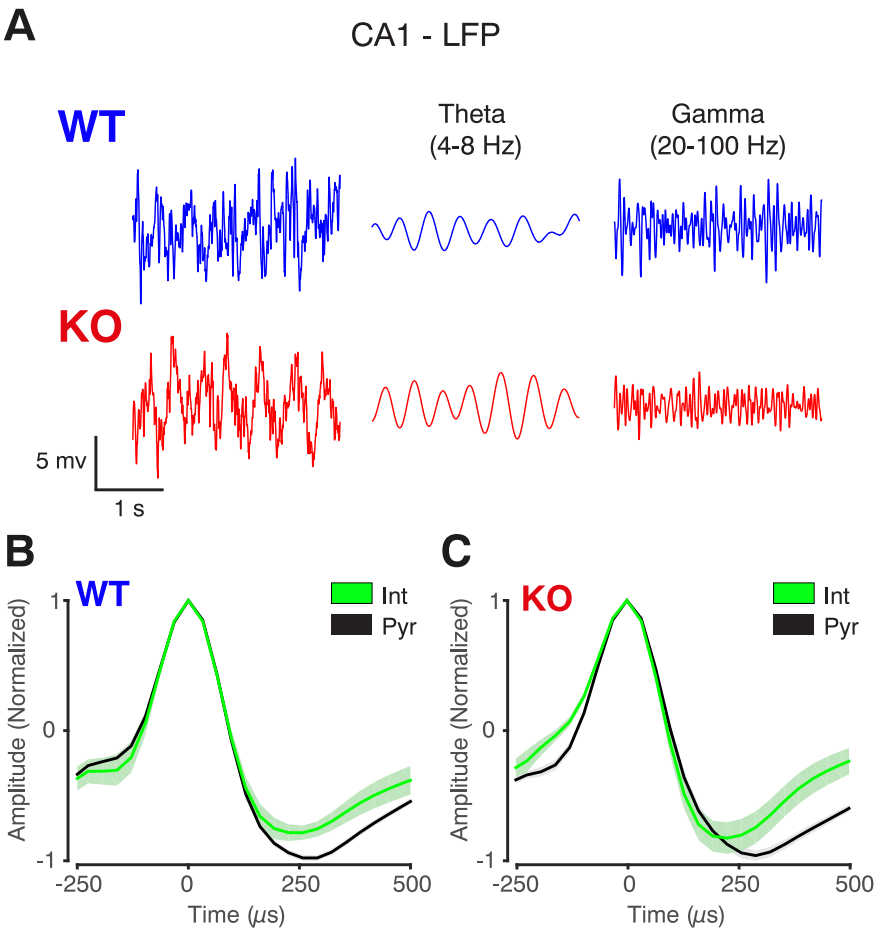

Fig. 2. LFP and neuronal recordings.
(A) Left, example CA1 LFP traces for WT and KO. Middle and right, same traces bandpass filtered for theta (4–8 Hz) and gamma (20–100 Hz) frequencies. (B) Normalized spike waveforms of pyramidal cells (Pyr, black) and interneurons (Int, green) for WT. (C) Same as in (B), for KO.

Table 1
Waveform parameters per genotype and neuronal type.

Genotype	Type	Mean AC (mean ± SEM) (ms)	ISVD (mean ± SEM) (mV/ms)	Peak-to-valley ratio (mean ± SEM)
WT	Interneurons	26.1 ± 0.4	41.5 ± 2.9	5.9 ± 1.3
	Pyramidal cells	20.5 ± 0.3	30.4 ± 0.8	2.8 ± 0.5
KO	Interneurons	24 ± 0.4	43.4 ± 3.1	1.7 ± 0.2
	Pyramidal cells	20.2 ± 0.3	31.4 ± 0.7	4.8 ± 0.8

$F_{1,350} = 2.02$, $p = 0.14$; peak-to-valley ratio: $F_{1,378} = 1.03$, $p = 0.31$). Therefore, proper comparisons between neuronal populations can be performed across genotypes.

We first evaluated firing rate differences between neuronal types and genotypes. We did not find significant firing rate differences of pyramidal cells and interneurons compared between genotypes (Fig. 3A: pyramidal cells, WT: 1.3 ± 0.1 Hz, KO: 1.1 ± 0.1 Hz, $p = 0.27$; interneurons, WT: 8.1 ± 1.1 Hz, KO: 8.9 ± 0.9 Hz, $p = 0.09$, Wilcoxon rank sum test), indicating that, despite the imbalance in excitatory/inhibitory ratio observed in *Fmr1*-KO mice in the first two postnatal weeks (Gonçalves et al., 2013), isolated spiking responses of CA1 neurons are unaffected in adult animals.

Previous reports have shown that *Fmr1*-KO mice exhibit higher neocortical excitability, expressed as an increased probability of neuronal firing (Gonçalves et al., 2013). An increased probability of neural firing disrupts spontaneous correlations among cell assemblies (Salinas et al., 2000). We therefore evaluated whether an imbalance in excitatory/inhibitory ratio might trigger CA1 hippocampal network aberrations, using spike-count correlations (r_{SC}), as a measure of the common variance between two neurons (Cohen and Kohn, 2011; Averbeck and Lee, 2006). First, we used a 0.5 s time window (consistent with the analysis time window used for spike-field comparisons) to bin CA1 spikes evoked during active movement through the arena, to then compute spike-count correlations between interneurons and pyramidal cells. We found no difference in r_{SC} between *Fmr1*-KO and WT pyramidal cell pairs. In contrast, pairs of *Fmr1*-KO interneurons, together with pyramidal cell-interneuron pairs, showed dramatically lower correlated spike-counts compared to WT (Fig. 3B: mean ± SEM r_{SC} pyramidal neurons comparison: WT: 0.055 ± 0.01 KO: 0.07 ± 0.01, $p = 0.10$, interneurons comparison: WT: 0.42 ± 0.05 KO: 0.12 ± 0.03 $p < 0.001$, pyramidal to interneurons comparison: WT: 0.07 ± 0.01 KO: 4×10^{-4} ± 0.01 $p < 0.001$, Wilcoxon rank sum test). Since spike-count correlations can be affected by bin-width (Kass and Ventura, 2006; Ventura et al., 2005), we controlled whether r_{SC} differences between genotypes can be observed across a wide range of bins (from 0.05 to 1 s). We observed a monotonic increase of r_{SC} values

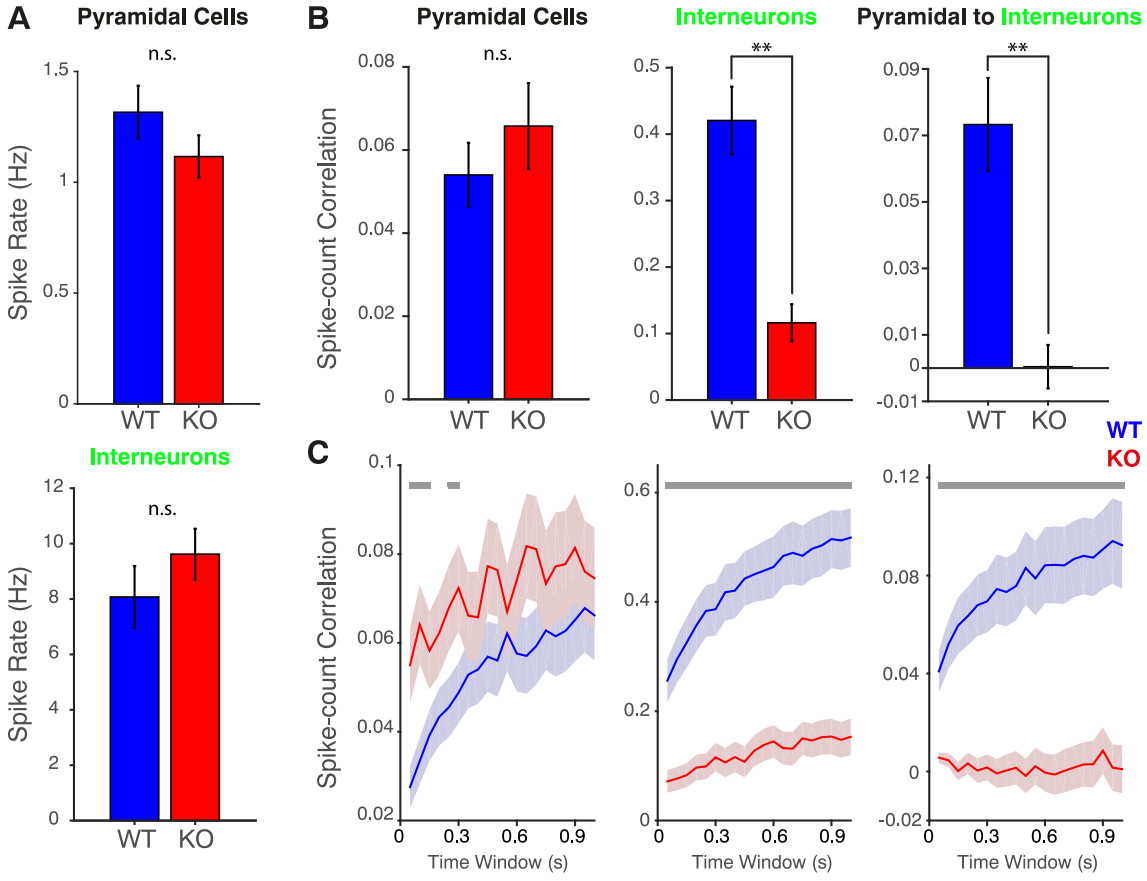

Fig. 3. Spike rates and spike-count correlations across different neuronal types.
(A) Average spike rate of CA1 pyramidal cells and interneurons for WT and KO. (B) CA1 WT and KO spike count correlations between pyramidal cells, interneurons, and mixed pyramidal cell-interneuron pairs calculated within 0.4 s time windows. (C) CA1 WT and KO spike count correlations between pyramidal cell, interneuron, and mixed pyramidal cell and interneuron pairs across varying time windows. Gray bar marks significant differences between genotypes (two-tailed $p < 0.05$, nonparametric randomization test across sessions).
Data are represented as mean ± SEM. **$p < 0.01$.

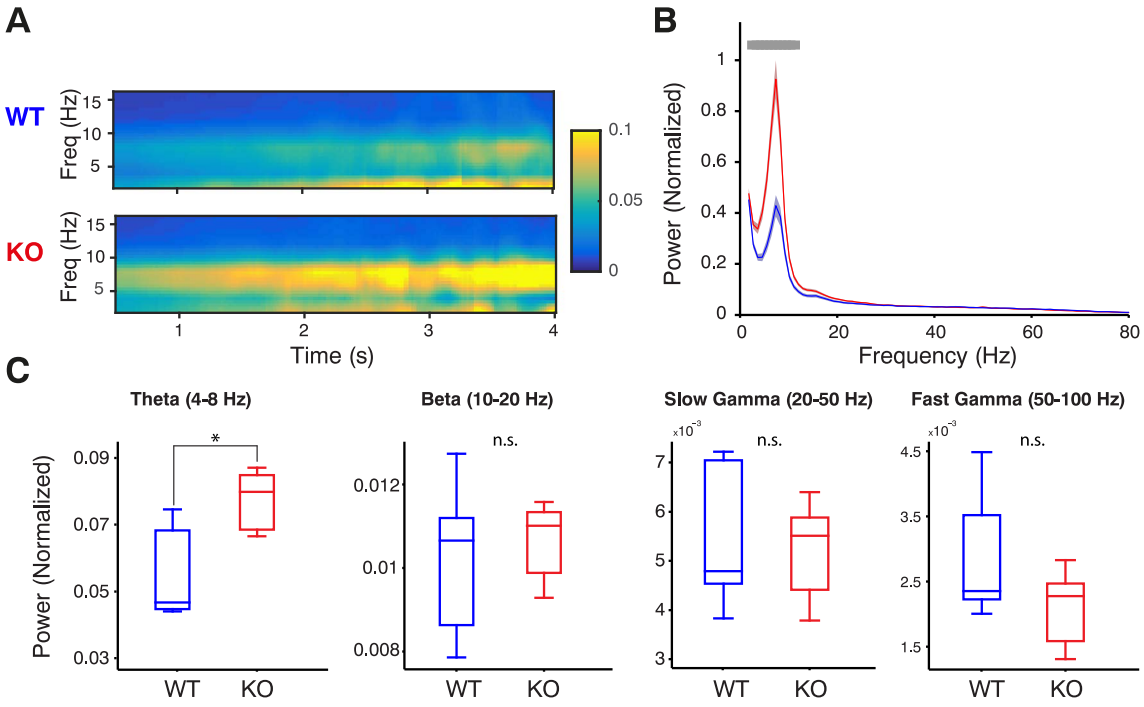

Fig. 4. LFP power.
(A) WT and KO time frequency power spectra of LFP recorded in hippocampal CA1, during the first 4 s of each continuous recorded segment in which the animal moved above threshold speed (3 cm/s). (B) Full spectrum CA1 LFP power for WT and KO mice. Gray bar marks significant differences between genotypes ($p < 0.05$). (C) Boxplot of WT and KO CA1 LFP power per frequency band. Data in (B) are represented as mean ± SEM. *$p < 0.05$.

associated with augmented counting window segments (Fig. 3C), which is particularly evident in all WT comparisons, but less prominent for all KO comparisons. This increase of r_{SC} values has been related to excess of variability in spike timing across trials (Nandy et al., 2017), which tends to be reduced with larger bins of observation (Richter et al., 2015). Nevertheless, spike-count correlations between interneurons and between interneurons and pyramidal cells of KO mice were not affected by the window selection. Differences between genotypes remain significant over a wide range of counting window segments (Fig. 3C: gray bar denotes a two-tailed p value < 0.05, nonparametric randomization test across recording sessions), indicative of a significant difference in the common variability between interneurons and between interneurons and pyramidal cells between both genotypes. These results confirm that synaptic dysfunctions caused by *Fmr1* protein deficits affect hippocampal circuit organization, decreasing the correlated variance between cell assemblies.

Next, we wondered whether the observed differences in hippocampal spike-count correlations are associated with other electrophysiological changes. Previous reports reveal the presence of two different gamma bands (slow (20–50 Hz) and fast (50–100 Hz)), both involved in the communication between CA1 and CA3 and between CA1 and entorhinal cortex (Colgin et al., 2009; Csicsvari et al., 2003; Bragin et al., 1995). We evaluated LFP power in theta, beta, slow, and fast gamma bands of the CA1 pyramidal cell layer during exploration. Both genotypes showed strong theta band LFP activity (Fig. 4A), but theta frequency power was significantly larger in *Fmr1*-KO than WT mice when compared across sessions (Fig. 4A and B: $p < 0.05$, non-parametric randomization test). This effect was preserved after compiling sessions and computing the average per animal (Fig. 4C: Theta band: median WT: 0.05, KO: 0.08, $p = 0.03$; Beta band: median WT: 0.01, KO: 0.01, $p = 0.54$; Slow Gamma band: median WT: 4.7×10^{-3}, KO: 5.5×10^{-3}, $p = 0.69$; Fast Gamma band: median WT: 2.3×10^{-3}, KO: 2.2×10^{-3}, $p = 0.22$, Wilcoxon rank sum test).

We did not find significant power differences in the slow and fast gamma band activity in CA1 between genotypes (Fig. 4C). However, power spectra can fail to reveal changes in rhythms that are detectable with metrics of LFP-LFP phase locking (Vinck et al., 2013; Brunet et al., 2014). Therefore, we quantified phase synchronization using the weighted phase lag index metric (WPLI, see Methods). *Fmr1*-KO mice showed increased phase synchronization in the slow gamma band across neighboring electrodes compared to WT (Fig. 5A: $p < 0.05$, non-parametric randomization test across sessions). This effect was preserved after compiling sessions and computing the average per animal (Fig. 5B: Theta WT: 0.69, KO: 0.86, $p = 0.68$; Beta WT: 0.37, KO: 0.59, $p = 0.34$; Slow Gamma WT: 0.47, KO: 0.89, $p = 0.02$; Fast Gamma WT: 0.71, KO: 0.72, $p = 0.34$, Wilcoxon rank sum test).

Finally, we evaluated the spike-LFP phase consistency (PPC) across different neuronal types in CA1. We calculated spike-triggered averages (STAs) of pyramidal cells and interneurons for both genotypes (Fig. 6A and B). Pyramidal cells of both genotypes showed a weak phase locking to a low (~10 Hz) frequency component of the LFP (Fig. 6A). Conversely, interneuron spikes of *Fmr1*-KO were more strongly locked to a low-frequency rhythm than WT interneurons (Fig. 6B). We calculated the pairwise phase consistency across frequencies (PPC, see Methods) (Vinck et al., 2010) to quantify these observations. Pyramidal cells of both genotypes showed a PPC spectra peaked at theta frequency (Malkki et al., 2016), but no significant differences between groups (Fig. 6C). Notably, *Fmr1*-KO interneurons locked to two frequency bands (5–8 Hz and 19–21 Hz) significantly stronger than those of WT mice (Fig. 6D: $p < 0.05$; non-parametric randomization test across sessions), suggesting an abnormal phase consistency for multi -frequency LFP rhythms in the *Fmr1*-KO mouse.

4. Discussion

In the present study, we took advantage of the spatial resolution provided by tetrode recordings in a mouse model of FXS to characterize how decreased FMRP expression affects CA1 hippocampal networks. We found increased theta power (5–8 Hz) associated with an increase of slow gamma (19–21 Hz) LFP-LFP synchronization in *Fmr1*-KO mice

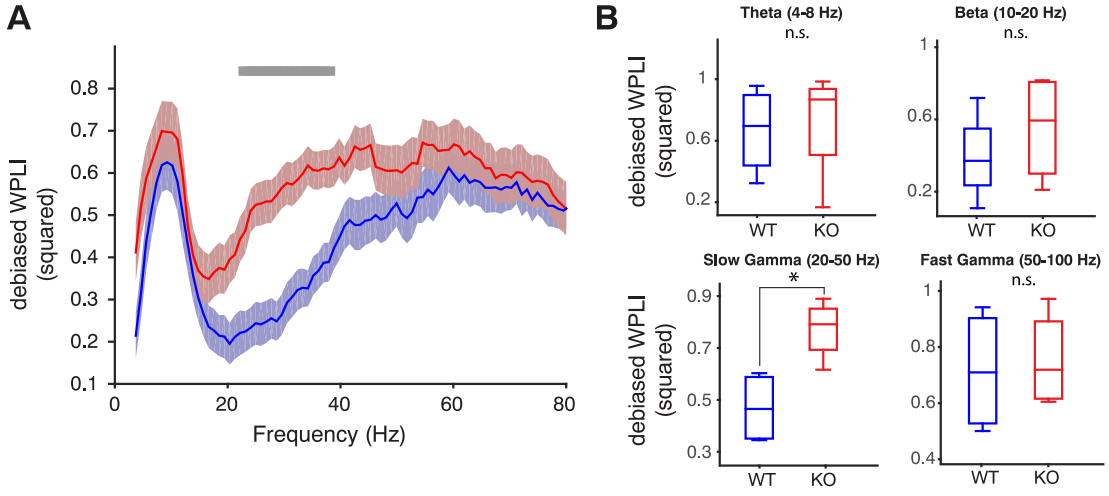

Fig. 5. LFP coherence.
(A) Full spectrum of LFP coherence (debiased WPLI) among tetrodes in WT (blue) and KO CA1 (red). Gray bar marks significant differences between genotypes ($p < 0.05$). Data are represented as mean ± SEM. (B) Boxplot of WT and KO CA1 LFP coherence per frequency band. *$p < 0.05$.

compared with WT controls, two findings that are consistent with pathological hypersynchronization of *Fmr1*-KO neurons to the most prominent hippocampal rhythm. Also, we observed decreased spike-count correlation in the *Fmr1*-KO mouse mainly across pairs of interneurons and pyramidal-interneurons, although it was also present between pyramidal cells at spike-counting windows below 0.3 s. A decrease in spike-count correlations has been linked to V4 cell assemblies during attention (Mitchell et al., 2009). Active states lead to a common variance reduction across connected neurons, which has been associated with increased phase-locking to specific LFPs oscillations (Womelsdorf et al., 2012). Our results suggest that FMRP deficits can be characterized by a hypersynchronized state between CA1 neurons.

Pathologically synchronized neuronal networks can account for several of the symptoms observed in FXS (Fung and Reiss, 2016). FXS patients show a major incidence of epilepsy and enhanced reactivity to sensory stimulation compared to normal subjects (Finelli et al., 1985; Sabaratnam et al., 2001), and abnormal fronto-parietal coherence in alpha, theta and beta frequency bands (van der Molen et al., 2014). Moreover, FXS patients exhibit increased resting-state gamma frequency band power, correlated with impaired social and sensory processing (Wang et al., 2017). This hypersynchronized state has also been found in animal models of FXS. In a FXS rat model, abnormal high-frequency power increases in association with decreased interneuronal firing-rate correlations have been observed in visual cortex during resting states (Berzhanskaya et al., 2017). Also, in the CA1 region of *Fmr1*-KO mice, an abnormal cross-frequency coupling between low and high-frequency LFP bands has been associated with cognitive inflexibility in a place-avoidance paradigm (Radwan et al., 2016). Experimental and modeling studies have shown that synchronized neuronal inputs cause increased excitability (Salinas et al., 2000; Azouz and Gray, 2000). In our study, *Fmr1*-KO mice exhibited increased theta power and gamma WPLI when compared with control mice, a finding that is consistent with increased microcircuit excitability in FXS (Berzhanskaya et al., 2017; Gonçalves et al., 2013). As gamma oscillations are nested in theta oscillations, this increased *Fmr1*-KO gamma synchronization might be driven by the increased power of the theta oscillations.

Hippocampal gamma oscillations in CA1 reflect mainly the weighted sum of postsynaptic inhibitory potentials from local interneurons, which homogenize and temporally align neuronal network

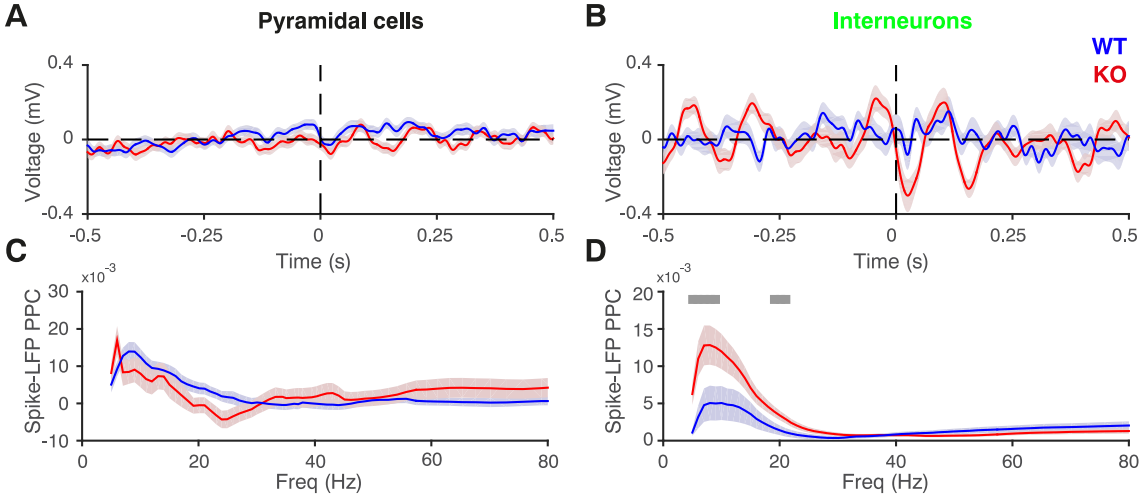

Fig. 6. Spike-triggered LFP average and spike-LFP consistency.
(A) Spike-triggered LFP average of WT and KO CA1 pyramidal cells. (B) Spike-triggered LFP average of WT and KO CA1 interneurons. (C) Pairwise Phase Consistency (PPC) of spike-LFP phase-locking of WT and KO CA1 pyramidal cells. (D) Consistency of spike-LFP phase-locking of WT and KO CA1 interneurons. Gray bars mark significant differences between genotypes ($p < 0.05$). Data are represented as mean ± SEM. *$p < 0.05$.

activity upon rhythmic input from CA3 (slow gamma) and entorhinal cortex (fast gamma) (Csicsvari et al., 2003). These two types of gamma activity appear to have functionally distinct roles: sensory signals carrying spatial information may be communicated from entorhinal cortex to CA1 through synchronization of fast gamma (suitable for inducing synaptic plasticity supporting consolidation of this information), whereas synchronization of CA1 to CA3 slow gamma occurs during memory retrieval (Colgin et al., 2009; Bieri et al., 2014). The increased phase consistency in CA1 slow gamma observed *Fmr1*-KO mice may suggest a preferential communication with the CA3 region (Colgin et al., 2009), reducing the effect of "on-line" inputs from entorhinal cortex and thus, overriding novel memory encoding mechanisms. This dysregulated communication may underlie deficits in spatial coding observed in these animals (Arbab et al., 2017).

Contrary to our results, Radwan and colleagues (Radwan et al., 2016) found minimal hippocampal CA1 power spectral differences between WT and *Fmr1*-KO. This discrepancy might be explained by differences in the behavioral protocols used in both studies. Radwan and colleagues (Radwan et al., 2016) used an active place avoidance protocol, producing behavioral differences across conditions and genotypes, but limiting free movement of the animals. Conversely, our recordings were obtained in animals freely moving in an open field, and no behavioral differences between genotypes were observed. Nevertheless, Radwan and colleagues (Radwan et al., 2016) also found abnormal rhythmic coupling in the hippocampus of *Fmr1*-KO.

In neocortex, FXS animal models show increased spiking activity (Berzhanskaya et al., 2017; Gonçalves et al., 2013). While our hippocampal recordings did not show spike rate differences between genotypes, we found significant differences in spike-count correlations between different cell types. Active neocortical states decorrelate spontaneous neuronal activity (Vinck et al., 2015; Renart et al., 2010; Montijn et al., 2015), possibly through coordinated fluctuations between excitatory and inhibitory populations (Renart et al., 2010). This uncorrelated state has been found in other studies. For instance, barrel cortex activity is actively desynchronized during active whisking (Poulet and Petersen, 2008) and visual cortical neurons show attention-dependent reduction in correlated low-frequency firing rate fluctuations (Mitchell et al., 2009; Hansen et al., 2012). In hippocampus, two-photon calcium imaging in CA1 neuronal populations has shown increased calcium event-count correlation of neuronal populations sharing common inputs (Modi et al., 2014). Once animals have been exposed to associative learning training, these spontaneous correlations tend to decrease and form separate clusters of correlated activity (Modi et al., 2014; Montijn et al., 2016). Thus, uncorrelated neuronal activity is important to efficiently transfer information across neuronal populations. At first glance, it seems counterintuitive that *Fmr1*-KO mice show decreased spike-count correlations compared with WT. However, this uncorrelated activity was observed together with an abnormal phase locking of interneurons to theta and slow gamma oscillations, and other studies have shown that increased spike phase-locking to gamma rhythm decreases noise correlations during visual stimulation in V1 cells (Womelsdorf et al., 2012). Possibly, synaptic deficits in *Fmr1*-KO may interfere with interneuron locking to the LFP, imposing an aberrant temporal precision to the activity of both pyramidal cells and interneurons in area CA1. In turn, this temporal precision, imposed on interneuron activity, may decrease the common variance across cells measured by spike-count correlations. Future studies will need to investigate whether this aberrant hippocampal activity affects hippocampus-dependent learning and memory consolidation processes in *Fmr1*-KO mice.

In conclusion, our results support the notion that deficits in FRMP produce an increased and pathological synchronization of CA1 neurons, probably because of an inadequate excitatory/inhibitory coupling between neurons, expressed in the theta and gamma ranges (Fenton, 2015). Hypersynchrony is thus not only related to neocortical activity, but is a more general feature of FXS, affecting both neocortical and hippocampal microcircuits.

Acknowledgements

We thank L. Noldus for the use of Ethovision XT software, K. Harris for the use of Klustakwik, and L. Hazan for the use of Klusters. This work was supported by SenterNovem BSIK grant 03053, STW grant AET7613, and EU project 720270 (HBP SGA1, Human Brain Project) to CMAP and the FLAG-ERA JTC 2015 project CANON (co-financed by NWO to CAB). Animals were kindly provided by Prof. Dr. R. Willemsen at the Department of Clinical Genetics, Erasmus MC in Rotterdam, The Netherlands.

Financial disclosures

The authors declare no competing financial interests.

References

Arbab, T., Pennartz, C.M.A., Battaglia, F.P., 2017. Impaired hippocampal representation of place in the Fmr1-knockout mouse model of fragile X syndrome. bioRxiv. http://dx.doi.org/10.1101/191775.
Averbeck, B.B., Lee, D., 2006. Effects of noise correlations on information encoding and decoding. J Neurophysiol 95, 3633–3644.
Azouz, R., Gray, C.M., 2000. Dynamic spike threshold reveals a mechanism for synaptic coincidence detection in cortical neurons in vivo. Proc Natl Acad Sci U S A 97, 8110–8115.
Battaglia, F.P., Kalenscher, T., Cabral, H., Winkel, J., Bos, J., Manuputy, R., et al., 2009. The lantern: an ultra-light micro-drive for multi-tetrode recordings in mice and other small animals. J Neurosci Methods 178, 291–300.
Belmonte, M.K., Bourgeron, T., 2006. Fragile X syndrome and autism at the intersection of genetic and neural networks. Nat Neurosci 9, 1221–1225.
Berzhanskaya, J., Phillips, M.A., Gorin, A., Lai, C., Shen, J., Colonnese, M.T., 2017. Disrupted cortical state regulation in a rat model of fragile X syndrome. Cereb Cortex 27, 1386–1400.
Bhakar, A.L., Dölen, G., Bear, M.F., 2012. The pathophysiology of fragile X (and what it teaches us about synapses). Annu Rev Neurosci 35, 417–443.
Bieri, K.W., Bobbitt, K.N., Colgin, L.L., 2014. Slow and fast γ rhythms coordinate different spatial coding modes in hippocampal place cells. Neuron 82, 670–681.
Bosman, C.A., Lansink, C.S., Pennartz, C.M.A., 2014. Functions of gamma-band synchronization in cognition: from single circuits to functional diversity across cortical and subcortical systems. Eur J Neurosci 39, 1982–1999.
Bosman, C.A., Schoffelen, J.-M., Brunet, N., Oostenveld, R., Bastos, A.M., Womelsdorf, T., et al., 2012. Attentional stimulus selection through selective synchronization between monkey visual areas. Neuron 75, 875–888.
Bragin, A., Jando, G., Nadasdy, Z., Hetke, J., Wise, K., Buzsáki, G., 1995. Gamma (40–100 Hz) oscillation in the hippocampus of the behaving rat. J Neurosci 15, 47–60.
Brunet, N., Vinck, M., Bosman, C.A., Singer, W., Fries, P., 2014. Gamma or no gamma, that is the question. Trends Cogn Sci 18, 507–509.
Budimirovic, D.B., Kaufmann, W.E., 2011. What can we learn about autism from studying fragile X syndrome? Dev Neurosci 33, 379–394.
Buzsáki, G., Anastassiou, C.A., Koch, C., 2012. The origin of extracellular fields and currents - EEG, ECoG, LFP and spikes. Nat Rev Neurosci 13, 407–420.
Buzsáki, G., Buhl, D.L., Harris, K.D., Csicsvari, J., Czéh, B., Morozov, A., 2003. Hippocampal network patterns of activity in the mouse. Neuroscience 116, 201–211.
Cohen, M.R., Kohn, A., 2011. Measuring and interpreting neuronal correlations. Nat Neurosci 14, 811–819.
Colgin, L.L., Denninger, T., Fyhn, M., Hafting, T., Bonnevie, T., Jensen, O., et al., 2009. Frequency of gamma oscillations routes flow of information in the hippocampus. Nature 462, 353–357.
Colgin, L.L., Moser, E.I., 2010. Gamma oscillations in the hippocampus. Physiology (Bethesda) 25, 319–329.
Contractor, A., Klyachko, V.A., Portera-Cailliau, C., 2015. Altered neuronal and circuit excitability in fragile X syndrome. Neuron 87, 699–715.
Csicsvari, J., Jamieson, B., Wise, K.D., Buzsáki, G., 2003. Mechanisms of gamma oscillations in the hippocampus of the behaving rat. Neuron 37, 311–322.
Darnell, J.C., Van Driesche, S.J., Zhang, C., Hung, K.Y.S., Mele, A., Fraser, C.E., et al., 2011. FMRP stalls ribosomal translocation on mRNAs linked to synaptic function and autism. Cell 146, 247–261.
Fenton, A.A., 2015. Excitation-inhibition discoordination in rodent models of mental disorders. Biol Psychiatry 77, 1079–1088.
Finelli, P.F., Pueschel, S.M., Padre-Mendoza, T., O'Brien, M.M., 1985. Neurological findings in patients with the fragile-X syndrome. J Neurol Neurosurg Psychiatry 48, 150–153.
Fries, P., 2015. Rhythms for cognition: communication through coherence. Neuron 88, 220–235.
Fung, L.K., Reiss, A.L., 2016. Moving toward integrative, multidimensional research in modern psychiatry: lessons learned from fragile X syndrome. Biol Psychiatry 80, 100–111.
Gonçalves, J.T., Anstey, J.E., Golshani, P., Portera-Cailliau, C., 2013. Circuit level defects in the developing neocortex of fragile X mice. Nat Neurosci 16, 903–909.

Gupta, A.S., van der Meer, M.A.A., Touretzky, D.S., Redish, A.D., 2012. Segmentation of spatial experience by hippocampal theta sequences. Nat Neurosci 15, 1032–1039.
Hansen, B.J., Chelaru, M.I., Dragoi, V., 2012. Correlated variability in laminar cortical circuits. 76, 590–602.
Harris, K.D., Henze, D.A., Csicsvari, J., Hirase, H., Buzsáki, G., 2000. Accuracy of tetrode spike separation as determined by simultaneous intracellular and extracellular measurements. J Neurophysiol 84, 401–414.
Hazan, L., Zugaro, M., Buzsáki, G., 2006. Klusters, NeuroScope, NDManager: a free software suite for neurophysiological data processing and visualization. J Neurosci Methods 155, 207–216.
Huber, K.M., Gallagher, S.M., Warren, S.T., Bear, M.F., 2002. Altered synaptic plasticity in a mouse model of fragile X mental retardation. Proc Natl Acad Sci U S A 99, 7746–7750.
Kass, R.E., Ventura, V., 2006. Spike count correlation increases with length of time interval in the presence of trial-to-trial variation. Neural Comput 18, 2583–2591.
Kass, R.E., Ventura, V., Brown, E.N., 2005. Statistical issues in the analysis of neuronal data. J Neurophysiol 94, 8–25.
Kates, W.R., Abrams, M.T., Kaufmann, W.E., Breiter, S.N., Reiss, A.L., 1997. Reliability and validity of MRI measurement of the amygdala and hippocampus in children with fragile X syndrome. Psychiatry Res 75, 31–48.
Kazdoba, T.M., Leach, P.T., Silverman, J.L., Crawley, J.N., 2014. Modeling fragile X syndrome in the Fmr1 knockout mouse. IRDR 3, 118–133.
Kim, J.J., Fanselow, M.S., 1992. Modality-specific retrograde amnesia of fear. Science 256, 675–677.
Lansink, C.S., Goltstein, P.M., Lankelma, J.V., Pennartz, C.M.A., 2010. Fast-spiking interneurons of the rat ventral striatum: temporal coordination of activity with principal cells and responsiveness to reward. Eur J Neurosci 32, 494–508.
Malkki, H.A.I., Mertens, P.E.C., Lankelma, J.V., Vinck, M., van Schalkwijk, F.J., van Mourik-Donga, L.B., et al., 2016. Effects of Arc/Arg3.1 gene deletion on rhythmic synchronization of hippocampal CA1 neurons during locomotor activity and sleep. Neurobiol Learn Mem 131, 155–165.
Manns, J.R., Hopkins, R.O., Reed, J.M., Kitchener, E.G., Squire, L.R., 2003. Recognition memory and the human hippocampus. Neuron 37, 171–180.
Maris, E., Schoffelen, J.-M., Fries, P., 2007. Nonparametric statistical testing of coherence differences. J Neurosci Methods 163, 161–175.
Markram, H., Lübke, J., Frotscher, M., Sakmann, B., 1997. Regulation of synaptic efficacy by coincidence of postsynaptic APs and EPSPs. Science 275, 213–215.
Mientjes, E.J., Nieuwenhuizen, I., Kirkpatrick, L., Zu, T., Hoogeveen-Westerveld, M., Severijnen, L., et al., 2006. The generation of a conditional Fmr1 knock out mouse model to study Fmrp function in vivo. Neurobiol Dis 21, 549–555.
Mitchell, J.F., Sundberg, K.A., Reynolds, J.H., 2009. Spatial attention decorrelates intrinsic activity fluctuations in macaque area V4. Neuron 63, 879–888.
Modi, M.N., Dhawale, A.K., Bhalla, U.S., 2014. CA1 cell activity sequences emerge after reorganization of network correlation structure during associative learning. Elife 3, e01982.
van der Molen, M.J.W., Stam, C.J., van der Molen, M.W., 2014. Resting-state EEG oscillatory dynamics in fragile X syndrome: abnormal functional connectivity and brain network organization. (F. J. Esteban, editor). PLoS One 9, e88451.
Montijn, J.S., Goltstein, P.M., Pennartz, C.M., 2015. Mouse V1 population correlates of visual detection rely on heterogeneity within neuronal response patterns. (D. C. Van Essen, editor). Elife 4, e10163.
Montijn, J.S., Meijer, G.T., Lansink, C.S., Pennartz, C.M.A., 2016. Population-level neural codes are robust to single-neuron variability from a multidimensional coding perspective. Cell Rep 16, 2486–2498.
Morris, R.G., Garrud, P., Rawlins, J.N., O'Keefe, J., 1982. Place navigation impaired in rats with hippocampal lesions. Nature 297, 681–683.
Moscovitch, M., Cabeza, R., Winocur, G., Nadel, L., 2016. Episodic memory and beyond: the hippocampus and neocortex in transformation. Annu Rev Psychol 67, 105–134.
Nandy, A.S., Nassi, J.J., Reynolds, J.H., 2017. Laminar organization of attentional modulation in macaque visual area V4. Neuron 93, 235–246.
Nichols, T.E., Holmes, A.P., 2001. Nonparametric permutation tests for functional neuroimaging: a primer with examples. Hum Brain Mapp 15, 1–25.
Oostenveld, R., Fries, P., Maris, E., Schoffelen, J.-M., 2011. FieldTrip: open source software for advanced analysis of MEG, EEG, and invasive electrophysiological data. Comput Intell Neurosci 2011, 156869.
Pilpel, Y., Kolleker, A., Berberich, S., Ginger, M., Frick, A., Mientjes, E., et al., 2009. Synaptic ionotropic glutamate receptors and plasticity are developmentally altered in the CA1 field of Fmr1 knockout mice. J Physiol 587, 787–804.
Poulet, J.F.A., Petersen, C.C.H., 2008. Internal brain state regulates membrane potential synchrony in barrel cortex of behaving mice. Nature 454, 881–885.
Quiroga, R.Q., Reddy, L., Kreiman, G., Koch, C., Fried, I., 2005. Invariant visual representation by single neurons in the human brain. Nature 435, 1102–1107.
Radwan, B., Dvorak, D., Fenton, A.A., 2016. Impaired cognitive discrimination and discoordination of coupled theta-gamma oscillations in Fmr1 knockout mice. Neurobiol Dis 88, 125–138.
Reiss, A.L., Lee, J., Freund, L., 1994. Neuroanatomy of fragile X syndrome: the temporal lobe. Neurology 44, 1317–1324.
Renart, A., La Rocha, De J., Bartho, P., Hollender, L., Parga, N., Reyes, A., Harris, K.D., 2010. The asynchronous state in cortical circuits. Science 327, 587–590.
Richter, C.G., Thompson, W.H., Bosman, C.A., Fries, P., 2015. A jackknife approach to quantifying single-trial correlation between covariance-based metrics undefined on a single-trial basis. Neuroimage 114, 57–70.
Sabaratnam, M., Vroegop, P.G., Gangadharan, S.K., 2001. Epilepsy and EEG findings in 18 males with fragile X syndrome. Seizure 10, 60–63.
Salinas, E., Salinas, E., Sejnowski, T.J., 2000. Impact of correlated synaptic input on output firing rate and variability in simple neuronal models. J Neurosci 20, 6193–6209.
Santos, A.R., Kanellopoulos, A.K., Bagni, C., 2014. Learning and behavioral deficits associated with the absence of the fragile X mental retardation protein: what a fly and mouse model can teach us. Learn Mem 21, 543–555.
Schoffelen, J.M., Oostenveld, R., Fries, P., 2005. Neuronal coherence as a mechanism of effective corticospinal interaction. Science 308, 111–113.
Sejnowski, T.J., Paulsen, O., 2006. Network oscillations: emerging computational principles. J Neurosci 26, 1673–1676.
Skaggs, W.E., McNaughton, B.L., 1996. Replay of neuronal firing sequences in rat hippocampus during sleep following spatial experience. Science 271, 1870–1873.
Ventura, V., Cai, C., Kass, R.E., 2005. Trial-to-trial variability and its effect on time-varying dependency between two neurons. J Neurophysiol 94, 2928–2939.
Vinck, M., Batista-Brito, R., Knoblich, U., Cardin, J.A., 2015. Arousal and locomotion make distinct contributions to cortical activity patterns and visual encoding. Neuron 86, 740–754.
Vinck, M., Oostenveld, R., van Wingerden, M., Battaglia, F., Pennartz, C.M.A., 2011. An improved index of phase-synchronization for electrophysiological data in the presence of volume-conduction, noise and sample-size bias. Neuroimage 55, 1548–1565.
Vinck, M., van Wingerden, M., Womelsdorf, T., Fries, P., Pennartz, C.M.A., 2010. The pairwise phase consistency: a bias-free measure of rhythmic neuronal synchronization. Neuroimage 51, 112–122.
Vinck, M., Womelsdorf, T., Buffalo, E.A., Desimone, R., Fries, P., 2013. Attentional modulation of cell-class-specific gamma-band synchronization in awake monkey area v4. 80, 1077–1089.
Wang, J., Ethridge, L.E., Mosconi, M.W., White, S.P., Binder, D.K., Pedapati, E.V., et al., 2017. A resting EEG study of neocortical hyperexcitability and altered functional connectivity in fragile X syndrome. J Neurodev Disord 9 (1) 2017. (9: 11).
Womelsdorf, T., Lima, B., Vinck, M., Oostenveld, R., Singer, W., Neuenschwander, S., Fries, P., 2012. Orientation selectivity and noise correlation in awake monkey area V1 are modulated by the gamma cycle. Proc Natl Acad Sci U S A 109, 4302–4307.
Zheng, C., Bieri, K.W., Hsiao, Y.-T., Colgin, L.L., 2016. Spatial sequence coding differs during slow and fast gamma rhythms in the hippocampus. Neuron 89, 398–408.